

# ZIF-8 membrane-based cryo-stripping of trace impurities towards electronic grade C<sub>3</sub>H<sub>6</sub> production

Received: 13 April 2025

Accepted: 28 April 2026

Cite this article as: Yu, K., Dong, Y., Ji, T. *et al.* ZIF-8 membrane-based cryo-stripping of trace impurities towards electronic grade C<sub>3</sub>H<sub>6</sub> production.

*Nat Commun* (2026). <https://doi.org/10.1038/s41467-026-72913-8>

Kunpeng Yu, Yachao Dong, Taotao Ji, Jiayu Liu, Shiya Gu, Jianzhong Yin, Xinyu He, Bin Zheng, Jiachen Wang, Yunlei Gao, Guillaume Maurin & Yi Liu

We are providing an unedited version of this manuscript to give early access to its findings. Before final publication, the manuscript will undergo further editing. Please note there may be errors present which affect the content, and all legal disclaimers apply.

If this paper is publishing under a Transparent Peer Review model then Peer Review reports will publish with the final article.

## **ZIF-8 membrane-based cryo-stripping of trace impurities towards electronic grade C<sub>3</sub>H<sub>6</sub> production**

Kunpeng Yu<sup>1#</sup>, Yachao Dong<sup>1#</sup>, Taotao Ji<sup>1#</sup>, Jiaxu Liu<sup>1#</sup>, Shiya Gu<sup>1</sup>, Jianzhong Yin<sup>1</sup>, Xinyu He<sup>1</sup>, Bin Zheng<sup>2</sup>, Jiachen Wang<sup>1</sup>, Yunlei Gao<sup>1</sup>, Guillaume Maurin<sup>3,4</sup>, Yi Liu<sup>1,5\*</sup>

ARTICLE IN PRESS

<sup>1</sup> State Key Laboratory of Fine Chemicals, Frontier Science Center for Smart Materials, School of Chemical Engineering, Dalian University of Technology, Dalian 116024, China

<sup>2</sup> College of Materials Science and Engineering, Xi'an University of Science and Technology, Xi'an 710054, China

<sup>3</sup> ICGM, Univ. Montpellier, CNRS, ENSCM, 34293 Montpellier, France

<sup>4</sup> Institut universitaire de France (IUF), France

<sup>5</sup> Dalian Key Laboratory of Membrane Materials and Membrane Processes, Dalian University of Technology, Linggong Road 2, Ganjingzi District, Dalian, 116024, China

# These authors contributed equally

\* Corresponding author: Yi Liu.  
Email: diligenliu@dlut.edu.cn

### Abstract

Electronic-grade (EG)  $C_3H_6$  represents an essential feedstock for semiconductor manufacturing, yet its purification remains energy-intensive due to the difficulty in removing trace  $C_3H_8$  impurities via conventional cryogenic distillation, which requires high pressure and low temperature operation conditions. In this study, we demonstrate efficient  $C_3H_6/C_3H_8$  separation under practical operation conditions using a ZIF-8 membrane prepared at near-freezing temperature. Gas permeation results show that the  $C_3H_6/C_3H_8$  separation factor (SF) increases as temperature decreases, reaching 607 at  $-40\text{ }^\circ\text{C}$  and remaining independent of operating pressure. Under industry-relevant conditions ( $-20\text{ }^\circ\text{C}$ , 3 bar), the membrane

achieved a SF of 362 with  $C_3H_6$  flux of  $135.3 \times 10^{-5}\text{ mol m}^{-2}\text{ s}^{-1}$ , enabling one-step reduction of  $C_3H_8$  from 2998 ppm to 8 ppm and complete removal of  $C_4H_{10}$  from polymer-grade  $C_3H_6$  feed. Adsorption-diffusion analysis reveals that enhanced separation at subfreezing temperature originates from increased diffusion selectivity caused by contraction and rigidification of ZIF-8 window. Process analysis further shows that integrating the membrane with distillation column can upgrade 99.5%  $C_3H_6$  to  $\sim 5\text{N}$  purity while reducing operating cost by 56.57% ( $1.34\text{ US\$ kg}^{-1}\text{ EG } C_3H_6$ ).

ARTICLE IN PRESS

## Introduction

In recent decades, hard mask (HM) has emerged in lithograph and dry etch processes to achieve high-precision and multi-layer semiconductor manufacturing, e.g., high-aspect-ratio channel etching in 3D NAND flash memory chip production<sup>1-2</sup>. Compared with conventional Si-containing HMs, amorphous carbon hard mask (*a*-C HM) offers the superiority of high etch selectivity, low extinction coefficient, low thermal stress, and easy cleaning with O<sub>2</sub> ashing<sup>3-5</sup>. C<sub>3</sub>H<sub>6</sub> has emerged as the most commonly utilized carbon precursor to deposit *a*-C HM via plasma-enhanced chemical vapor deposition, owing to its superior deposition rate and uniformity<sup>6-8</sup>. However, a variety of co-existing impurities (Table S1) in polymer-grade C<sub>3</sub>H<sub>6</sub> (~99.5%) are detrimental to the deposition of homogeneous *a*-C HM<sup>9-10</sup>. To satisfy the stringent demands of microchip manufacturing, the purity of electronic grade (EG) C<sub>3</sub>H<sub>6</sub> should be at least higher than 99.99% (~4N) with the content of uppermost impurity of high-affinity C<sub>3</sub>H<sub>8</sub> no higher than 80 ppm, which demands meticulous stripping of ~3000 ppm C<sub>3</sub>H<sub>8</sub> in the feed stock.

Cryogenic distillation, which represents the dominant process for purifying EG C<sub>3</sub>H<sub>6</sub>, commonly involves removal of light impurities (abbreviated as de-light) including N<sub>2</sub> and C<sub>2</sub>H<sub>6</sub><sup>11-13</sup>, followed by removal of heavy impurities (abbreviated as de-heavy) comprising C<sub>3</sub>H<sub>8</sub> and *n*-/*i*-C<sub>4</sub>H<sub>10</sub><sup>14-15</sup>. However, deep stripping of co-existing C<sub>3</sub>H<sub>8</sub> commonly requires multiple rectification or coupling with other separation processes such as adsorption and extraction, incurring huge separation costs and low production efficiency<sup>16-18</sup>. Alternatively, membrane-based

separation features the superiority of low energy consumption, low capital cost, small footprint, and easy operation<sup>19-24</sup>. According to recent process modelling analyses, C<sub>3</sub>H<sub>6</sub>/C<sub>3</sub>H<sub>8</sub> separation membranes with selectivity higher than 100 could offer 90% energy savings compared with distillation<sup>25-28</sup>, which inspired us to integrate membrane process into EG C<sub>3</sub>H<sub>6</sub> production towards better economic proficiency and operational simplicity, i.e., replacing multi-stage de-heavy columns with single-stage membrane unit<sup>29-33</sup>.

As complementary to polymeric membranes, molecular sieve membranes have shown great potential in accurate discrimination of gas mixtures with subtle discrepancy in kinetic diameters<sup>34-38</sup>, which offers a facile process for the removal of heavy impurities with kinetic diameters larger than C<sub>3</sub>H<sub>6</sub><sup>39-42</sup>. In terms of C<sub>3</sub>H<sub>6</sub>/C<sub>3</sub>H<sub>8</sub> separation, ZIF-8 membrane is regarded as one of the most promising candidates owing to its inherent framework flexibility, allowing permeation of C<sub>3</sub>H<sub>6</sub> at least 130 times faster than that of C<sub>3</sub>H<sub>8</sub> and other

bulky impurities<sup>43-49</sup>. It should be noted that although previous studies had validated the promises of ZIF-8 membranes in high-efficiency C<sub>3</sub>H<sub>6</sub>/C<sub>3</sub>H<sub>8</sub> separation under certain conditions, a majority of them were performed under ambient temperature and pressure with C<sub>3</sub>H<sub>6</sub> feed content in the range of 10-90% in the presence of sweep gas<sup>50-56</sup>. Regarding practical EG C<sub>3</sub>H<sub>6</sub> production, however, the bottom stream of de-light column is commonly occupied with saturated C<sub>3</sub>H<sub>6</sub> at temperature of -20 °C and pressure of 3 bar in the presence of trace amounts of heavy impurities (<0.5%). The performance of ZIF-8 membranes in high-efficiency C<sub>3</sub>H<sub>6</sub>/C<sub>3</sub>H<sub>8</sub> separation under practical operation conditions still remains largely unexplored so far. To meet the challenge of EG C<sub>3</sub>H<sub>6</sub> production, fabrication of ZIF-8 membranes capable of maintaining superior and stable C<sub>3</sub>H<sub>6</sub>/C<sub>3</sub>H<sub>8</sub> separation performance under subfreezing operation temperature, elevated operation pressure, extreme C<sub>3</sub>H<sub>6</sub> feed ratio, and evacuation operation conditions has become indispensable.

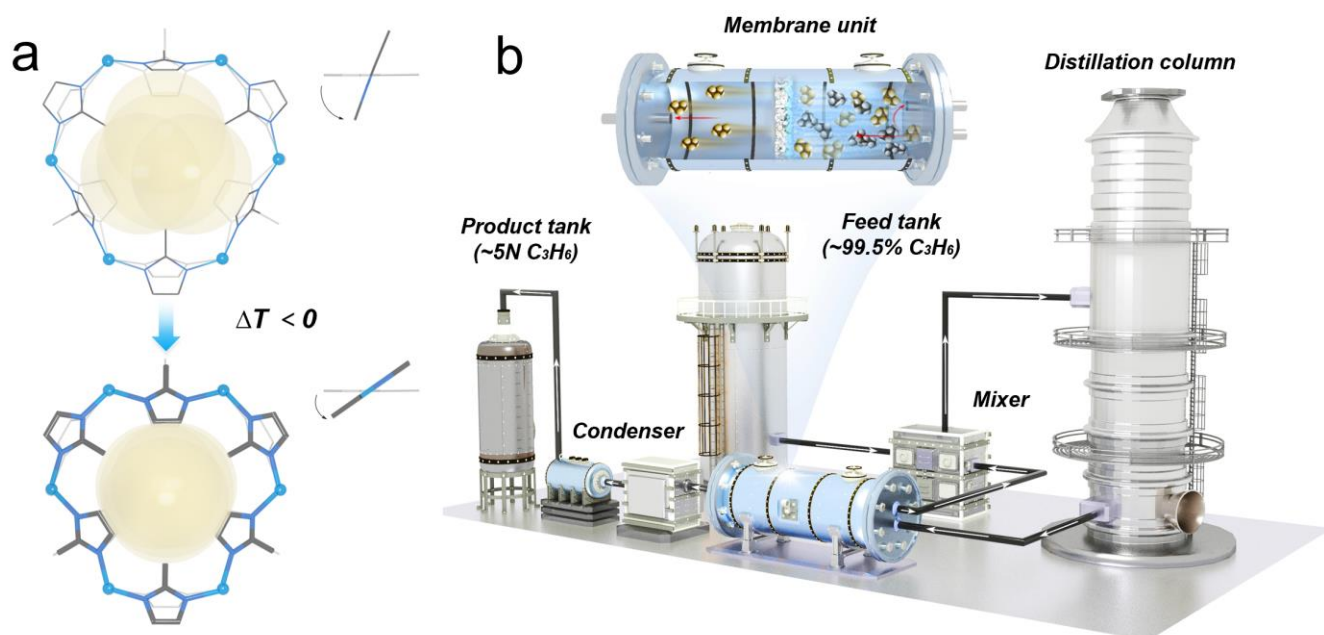


**Figure 1. Concept of low-temperature ZIF-8 membrane sieving and membrane-distillation hybrid process.** (a) Illustration of the low-temperature induced moderate contraction and rigidification of six-membered sieving windows of the ZIF-8 framework, and (b) schematic diagram of ZIF-8 membrane-distillation hybrid system for producing electronic grade C<sub>3</sub>H<sub>6</sub>.

Recently we developed a near-freezing protocol to prepare highly  $C_3H_6$ -permselective ZIF-8 membrane featuring exceptional and stable  $C_3H_6/C_3H_8$  separation performance at operation pressure up to 7 bar and  $C_3H_8$  feed percentage down to 1%<sup>57-59</sup>, relying on precisely controlled membrane growth kinetics and semi-confined membrane structure. Herein, we aimed to explore the  $C_3H_6/C_3H_8$  separation performance of ZIF-8 membrane under unprecedented extreme operation conditions in the context of practical EG  $C_3H_6$  production. Its  $C_3H_6/C_3H_8$  separation performance at sub-freezing temperature was first systematically investigated. Our results revealed that separation factor (SF) of equimolar  $C_3H_6/C_3H_8$  gas mixture increased steadily with decreasing operation temperature, even exceeding 600 at  $-40$  °C. This phenomenon was assigned to the slight contraction and rigidification of the six-ring membered gate size of the ZIF-8 framework upon decreasing operation temperature (Figure 1a) as revealed by a combination of spectroscopy and molecular simulations, resulting in significantly enhanced diffusion resistance of the bulky  $C_3H_8$  as demonstrated by gas diffusion rate studies. Subsequently, with polymer-grade  $C_3H_6$  as feedstock, gas permeation test was conducted at  $-20$  °C and 3 bar under vacuum operation to mimic the stripping of heavy impurities under industry-relevant operation conditions. Our membrane was demonstrated to enable one-step stripping of  $C_3H_8$  impurity from 2998 to 8 ppm accompanying with complete removal of trace amounts of *n*-*i*- $C_4H_{10}$  impurities. Finally, an idealized ZIF-8 membrane-cryogenic distillation coupling system was established for energy-efficient production of EG  $C_3H_6$  (Figure 1b). Process design analysis demonstrated that in comparison with conventional distillation, membrane-distillation hybrid system not only enabled high-efficiency production of high-standard EG  $C_3H_6$  ( $\sim 5N$ ) but also achieved significant reduction in operation cost (56.57%) and energy duty (49.89%), enabling energy-efficient and cost-saving EG  $C_3H_6$  production under practical operation conditions.

## Results

### Heavy impurities stripping under practical conditions

As mentioned in our previous work, near-freezing synthetic protocol was adopted to prepare highly  $C_3H_6$ -permselective ZIF-8 membrane. The preparation and characterization methods have been described in detail in Supplementary Methods. First, uniform ZnO buffer layer comprising 20 nm-sized ZnO grains (Figure 2a), which served as Zn source to facilitate heterogeneous ZIF-8 nucleation, was deposited on the surface of porous  $\alpha$ - $Al_2O_3$  substrate. Aiming at better control of nucleation and growth kinetic of the ZIF-8 membrane, cryo-

conversion reaction was performed on ZnO buffer layer-modified substrate. SEM results revealed that after reaction, the substrate surface had been uniformly covered with well-intergrown ZIF-8 crystallites with thickness of  $\sim 700$  nm (Figure 2b and d). X-ray diffraction (XRD) patterns confirmed that the conversion rate of ZnO buffer layer reached 83% (Figure 2c). EDXS surveys revealed that the overall thickness of the so-obtained ZIF-8 membrane was only  $1.2$   $\mu m$  as evidenced by the distribution of C element in cross-sectional region (Figure 2e), indicating a penetration depth of  $\sim 500$  nm embedded with unconverted ZnO buffer layer. This semi-confined microstructure (Figure 2f-h) not only reinforced binding strength and structural robustness, but also formed a space-constraint effect to prevent pressure-induced framework deformation, facilitating well preservation of the membrane performance under varying operation conditions. Corresponding AFM characterization demonstrated high surface flatness of the membrane ( $R_a=136$  nm, Figure S1).

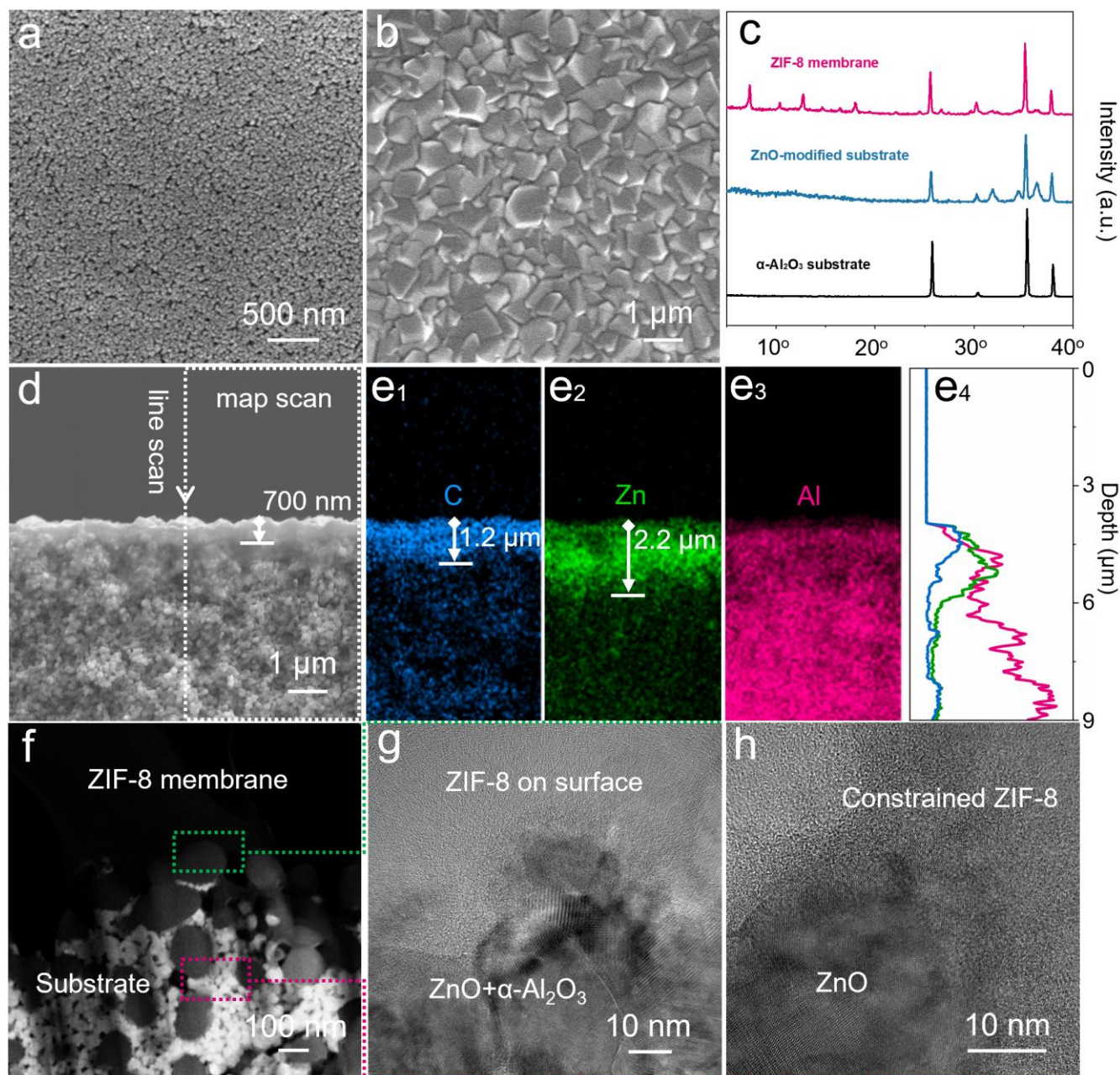


**Figure 2. Microstructural characterization of ZIF-8 membrane.** SEM images of (a) ZnO buffer layer-modified substrate, (b) near-freezing synthetic ZIF-8 membrane and (c) relevant XRD patterns. (d) Cross-sectional SEM image and (e) EDXS spectra of near-freezing synthetic ZIF-8 membrane. (f) FIB-assisted HAADF-STEM image and (g-h) corresponding HR-TEM images of semi-confined ZIF-8 membrane.

Aiming at  $C_3H_6$  purification in industry, the stripping ability of our membrane towards heavy impurities (mainly  $C_3H_8$  and  $n$ -/ $i$ - $C_4H_{10}$ ) was further measured under practical operation conditions. To couple with discharge conditions of the front de-light column, the separation performance of ZIF-8 membrane for an equimolar  $C_3H_6/C_3H_8$  gas mixture was first measured at varying operation temperature and pressure using the Wicke-Kallenbach method (Figure S2a and Supplementary Methods). The gas permeation results indicated that under atmospheric conditions, the  $C_3H_8$  permeance dropped more quickly upon decreasing operation temperature, resulting in steady elevation of  $C_3H_6/C_3H_8$  SF up to 607 at near-liquefaction temperature of  $-40\text{ }^\circ\text{C}$  (Figure 3a), which was superior to presently reported values in the literature (Figure S3 and Table S2-7). At practical discharge temperature of de-light column ( $-20\text{ }^\circ\text{C}$ ), the SF remained as high as 377, which had fully met the purity criteria of EG  $C_3H_6$  with no compromise in  $C_3H_6$  permeance.

Subsequently, the dependence of  $C_3H_6/C_3H_8$  separation performance of the so-obtained membrane on feed pressure was evaluated at industry-relevant  $-20\text{ }^\circ\text{C}$ . As shown in Figure 3b, with saturation pressure of 3 bar as threshold, the pressurization process could be divided into two stages: At the initial stage (from 1 to 3 bar), permeation flux of gaseous  $C_3H_6$  increased from  $74.1 \times 10^{-5}$  to  $135.3 \times 10^{-5}$  mol  $m^{-2}$   $s^{-1}$ , while further increasing feed pressure to 7 bar led to constant  $C_3H_6$  flux due to the liquefaction of  $C_3H_6/C_3H_8$  mixture at the feed side. Of particular note, regardless of pressure variation, our ZIF-8 membrane displayed constant  $C_3H_6/C_3H_8$  SF of about  $\sim 370$ . This well preservation of the  $C_3H_6/C_3H_8$  separation performance at elevated pressure might be ascribed to space constraint effect imposed by ZnO grain-embedded substrate pores. It should be noted that compared with ambient operation conditions, both  $C_3H_6/C_3H_8$  SF and  $C_3H_6$  flux throughout our membrane increased 1.89 and 1.22 times at discharge conditions (i.e.,  $-20\text{ }^\circ\text{C}$  and 3 bar) of de-light column, which enabled their direct coupling without extensive heat exchange and depressurization. Compared with conventional multi-stage cryogenic distillation process, this membrane-distillation hybrid system holds great potential in high-efficiency production of qualified EG  $C_3H_6$ .

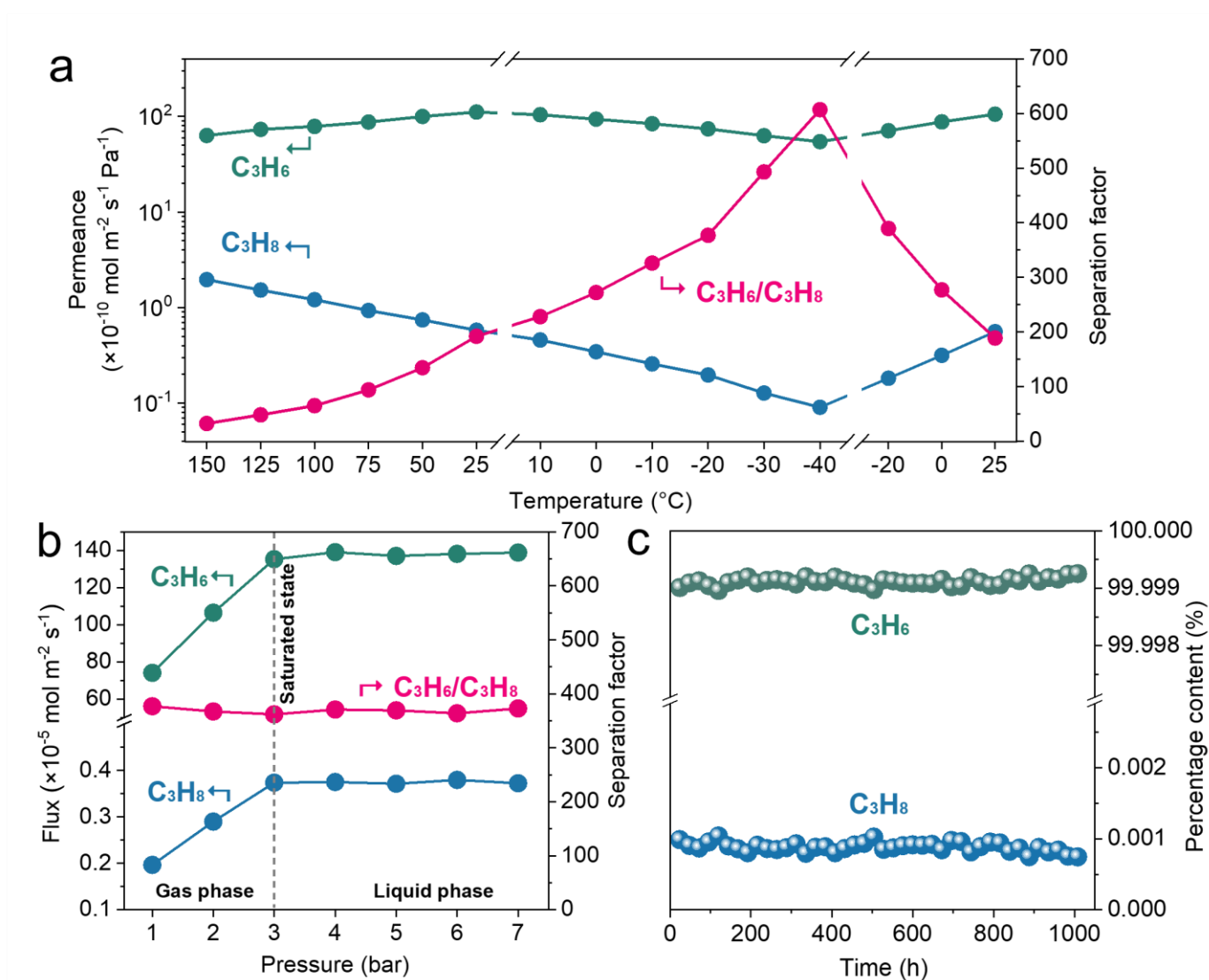


**Figure 3.  $C_3H_6/C_3H_8$  separation performance of ZIF-8 membrane.** (a) The dependence of  $C_3H_6/C_3H_8$  separation performance of ZIF-8 membrane on operation temperature (from 150 to  $-40$  °C) at atmospheric pressure. (b) The dependence of  $C_3H_6/C_3H_8$  separation performance of ZIF-8 membrane on operation pressure at industry-relevant temperature of  $-20$  °C. (c) Long-term operation stability of ZIF-8 membrane with polymer-grade  $C_3H_6$  as feedstock under  $-20$  °C, 3 bar and vacuum operation.

To further verify the stripping capability of our membrane towards heavy impurities under practical conditions, the membrane upstream feed was replaced with commercial 99.5% polymer-grade  $C_3H_6$  containing heavy impurities of 2998 ppm  $C_3H_8$ , 291 ppm  $n-C_4H_{10}$  and 203 ppm  $i-C_4H_{10}$ ; moreover, evacuation was applied at the permeate side with operation temperature and pressure maintained at industry-relevant  $-20\text{ }^\circ\text{C}$  and 3 bar, respectively (Figure S2b). Gas permeation results revealed that our membrane still maintained superior and stable  $C_3H_6/C_3H_8$  separation performance with  $C_3H_6/C_3H_8$  SF of 362 and  $C_3H_6$  flux of  $135.3 \times 10^{-5}$  mol  $m^{-2} s^{-1}$  (Figure S3). In terms of heavy impurity tripping,  $C_3H_8$  content in the permeate gas sharply reduced to less than 10 ppm with large-sized  $n/i-C_4H_{10}$  content falling below GC detection limit (Table S8). Of particular note, in the case of the presence of only heavy impurities, the  $C_3H_6$  purity in the permeate side reached 5N (99.999%) during 1000 h of continuous testing (Figure 3c). To further verify the long-term stability of prepared ZIF-8 membrane, we supplemented polymer-grade  $C_3H_6$  (~99.5%) from different gas suppliers as raw materials and conducted continuous tests for 200 h (Figure S4 and Table S9). Obviously, the purity of  $C_3H_6$  in the penetrant side still fully met the purity requirement (>5N). Therefore, our membrane is a highly effective alternative to traditional de-heavy column with potential advantages in terms of lower energy consumption and reduced capital cost.

#### Separation mechanism elucidation at lower temperature

The mechanism of enhanced  $C_3H_6/C_3H_8$  separation performance of our membrane at lower temperature was further elucidated. It is well established that  $C_3H_6$  and  $C_3H_8$  permeation behaviors in ZIF-8 framework conform to adsorption or diffusion-based mechanisms. Initially, static adsorption properties of  $C_3H_6$  and  $C_3H_8$  in ZIF-8 framework were investigated. It was observed that the equilibrium adsorption capacity of  $C_3H_6$  gradually increased and became higher than that of  $C_3H_8$  upon decreasing the temperature from  $75\text{ }^\circ\text{C}$  to  $-40\text{ }^\circ\text{C}$  (Figure S5-6), resulting in higher amount of equilibrium  $C_3H_6$  uptake and increasing  $C_3H_6/C_3H_8$  Ideal Adsorbed Solution Theory (IAST) selectivity (Figure 4a). Furthermore,  $C_3H_6$  and  $C_3H_8$  diffusion coefficients in ZIF-8 were estimated from *Langmuir* and *Dual-site Langmuir* model-fitted adsorption parameters in conjunction with gas permeation data<sup>60-61</sup> (Figure S7 and Table S10). As shown in Figure 4b, both  $C_3H_6$  and  $C_3H_8$  diffusion coefficients dropped quickly with decreasing temperature; however, the reduction in diffusion coefficient for  $C_3H_8$  was more prominent than for  $C_3H_6$ , resulting in a 5.7-fold increase in their diffusion

selectivity. Possibly this could be ascribed to low-temperature-induced reduction of the gate size, resulting in more pronounced increase in energy barrier for larger-sized  $C_3H_8$  to diffuse through the contracted and rigidified six-membered window<sup>62-63</sup>.

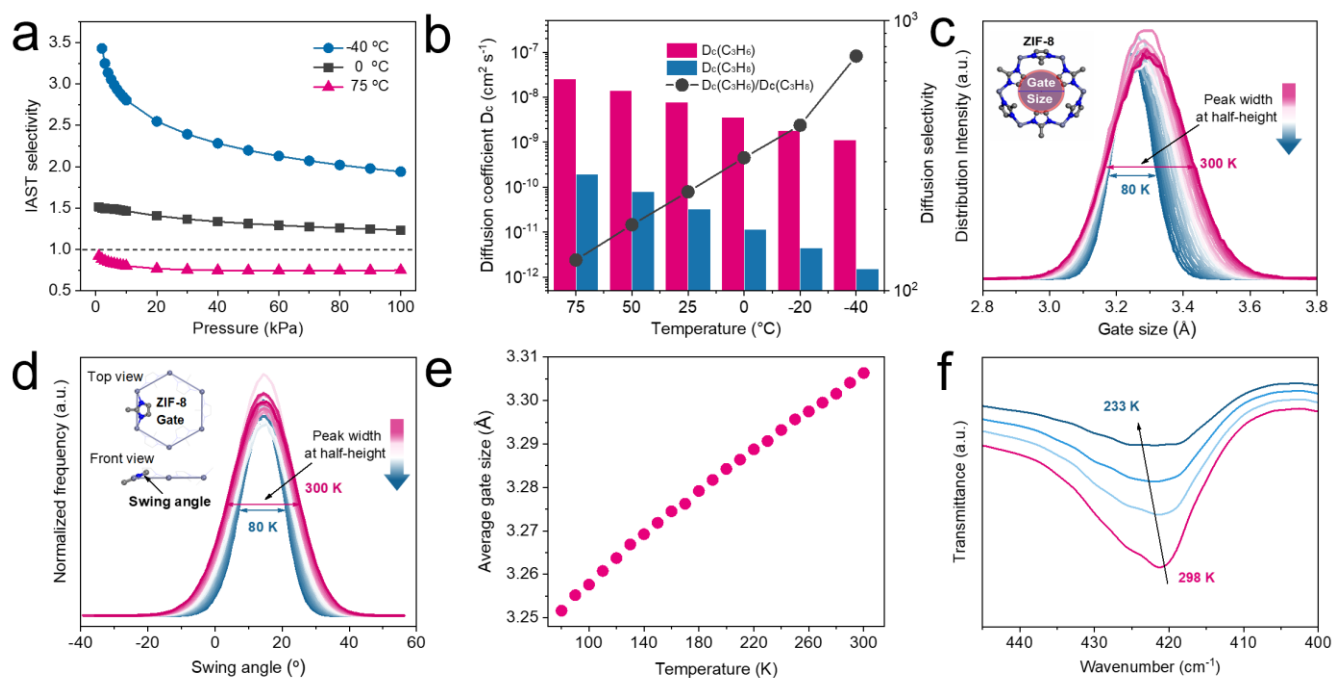


**Figure 4. Demonstration of rigidification effect in ZIF-8 framework caused by temperature reduction.** (a)  $\text{C}_3\text{H}_6/\text{C}_3\text{H}_8$  IAST adsorption selectivity of ZIF-8, the dashed line represents a selectivity of 1.0. (b) Diffusion coefficients of  $\text{C}_3\text{H}_6$  and  $\text{C}_3\text{H}_8$  in ZIF-8 framework and their diffusion selectivity calculated from gas adsorption parameters and permeation data. (c) Molecular dynamics simulated gate size distribution of ZIF-8, the gate size region is shown in inset figure. (d) Simulated swing angle distribution of the imidazolate linkers in ZIF-8 framework, the inset illustrates the temperature-dependent rotational motion of linkers. (e) Average gate size of ZIF-8 as a function of temperature obtained from molecular dynamics simulations. (f) In situ FT-IR spectra of ZIF-8 at different temperatures. As the test temperature decreases, the absorption peak blue-shifted to higher frequencies along the arrow direction.

To validate this hypothesis, flexible force field-based Molecular Dynamics simulations were carried out to explore how the gate size of ZIF-8 behaves at low temperature. These simulations revealed that the distributions of both gate size (Figure 4c) and swing angle (Figure 4d) for the imidazolate linkers becomes narrower when temperature decreases, supporting a rigidification of the six-membered rings. Accordingly, the averaged gate size slightly reduces when temperature decreases (Figure 4e). These trends strongly suggest that the gate crossing is harder for the bulkier  $C_3H_8$  vs  $C_3H_6$  at low temperature which is in line with the increase of diffusion-driven selectivity observed experimentally. Simultaneously, in situ FT-IR characterization was conducted to study the temperature-dependence of the rigidity of ZIF-8 framework. As shown in Figure 4f and S8, we observe that the absorption band at  $422\text{ cm}^{-1}$  that can be assigned to the Zn-N stretching vibration or the bending vibration between methyl group and imidazolate ring<sup>64</sup>, has a much lower intensity and is also blue-shifted to higher frequencies with decreasing temperature, which suggests an enhancement of the ZIF-8 framework rigidity at low temperature since higher energy is required to induce aforementioned bond vibrations<sup>65</sup>.

Enhanced kinetic sieving of ZIF-8 membrane at low temperature was further confirmed for the  $C_2H_4/C_2H_6$  separation, showing increased SF from 2.5 to 4.9 upon decreasing operation temperature from RT to  $-40\text{ }^\circ\text{C}$  (Figure S9 and Table S11). Overall, synergistic effect of adsorption and diffusion kinetics at lower temperature concurrently contributed to higher sieving precision towards  $C_3H_6/C_3H_8$  gas pair, which not only enhanced the separation efficiency and product purity, but also achieved a direct coupling between membrane unit and de-light column under identical operation conditions, holding great promise in reducing energy consumption and capital cost during EG  $C_3H_6$  production.

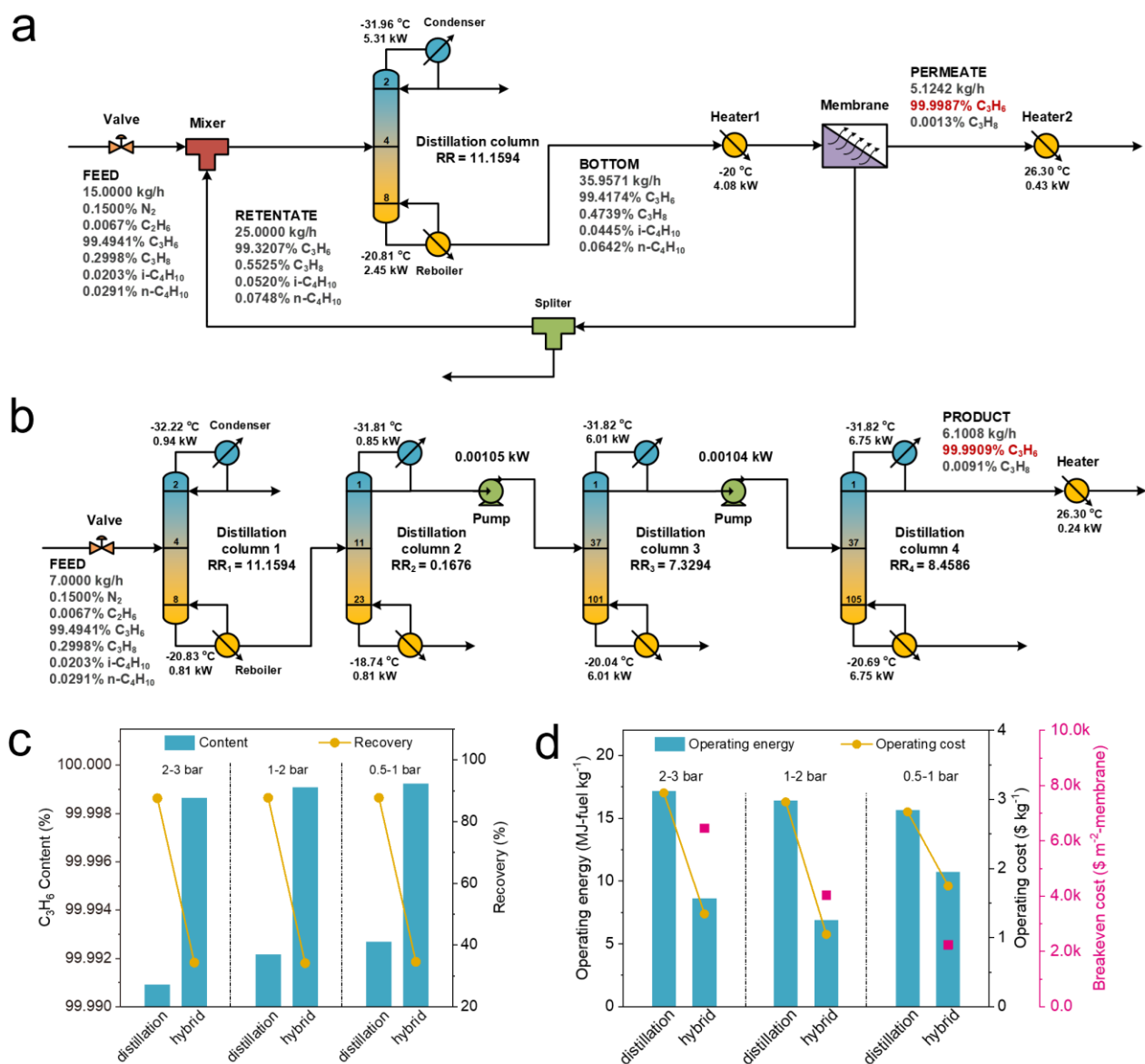


**Figure 5. Membrane-distillation hybrid system process and operating performance comparison.** Process flow diagram of (a) hybrid membrane-distillation system and (b) conventional cryogenic distillation system for EG C<sub>3</sub>H<sub>6</sub> purification with column pressure range of 2-3 bar. The comparisons of (c) product purity and recovery, (d) capital cost and operation cost.

### Process design analysis of membrane-based EG C<sub>3</sub>H<sub>6</sub> purification

To better evaluate practical operation in industry, we utilized a steady-state simulation model developed in Aspen Plus V11 software to conduct process simulations. The feedstock considered in this study is polymer-grade C<sub>3</sub>H<sub>6</sub>, therefore, adsorption steps (typically used as dryers or guard beds to remove trace polar impurities) were not explicitly modeled, as they do not represent a major contributor to the overall energy consumption for deep de-heavy separation. To explore the performance of the hybrid membrane-distillation system for separating C<sub>3</sub>H<sub>6</sub>/C<sub>3</sub>H<sub>8</sub> gas mixtures at different feed temperature and pressure, we simulated the hybrid membrane-distillation processes under three modes of 2-3 bar, 1-2 bar and 0.5-1 bar, depending on the feed pressure of columns (Figure S10). The Redlick-Kwong-Soave property method was selected, and the distillation column was simulated using the RadFrac model<sup>66</sup>. As a base scenario, we first modelled the hybrid membrane-distillation process employing polymer-grade C<sub>3</sub>H<sub>6</sub> as the raw material and targeting at C<sub>3</sub>H<sub>6</sub> purity exceeding 99.99%, in which the distillation column acted to remove light impurities including non-condensable gases and C<sub>2</sub>H<sub>6</sub><sup>67-68</sup>. Simultaneously, 25 m<sup>2</sup> ZIF-8 membrane was employed to strip the heavy impurities in the bottom product of the column. To enhance C<sub>3</sub>H<sub>6</sub> recovery, the retentate of the membrane was partially recycled back into the distillation column. For comparison, conventional distillation process (Figure S11) and another type of hybrid membrane distillation process based on membrane pre-treatment (Figure S12) were also modelled based on similar C<sub>3</sub>H<sub>6</sub> production capacity and operation pressure of the column.

After stream conditions relief to 3 bar and -20.81 °C from 1.2 MPa and 23.71 °C through the valve, the feedstock was introduced into the 9-tray distillation column from tray number 4 in the hybrid membrane-distillation system, with a top pressure of 2 bar and a bottom pressure of 3 bar, respectively. Considering the membrane processing capacity given above, the total feed rate of the column was originally set at 40.0 kg h<sup>-1</sup>, with a production target of 5.0 kg h<sup>-1</sup> of EG C<sub>3</sub>H<sub>6</sub>. Following the distillation column, our ZIF-8 membrane was further simulated with the standard component separator model. Separation parameters were determined by experimental data of gas permeation test with C<sub>3</sub>H<sub>6</sub>/C<sub>3</sub>H<sub>8</sub> SF of 362 (Table S12). The permeate gas came out of the membrane at 1 kPa, and the retentate part came out at feed pressure of 3 bar. Part of the retentate was removed from the process, which could still be used as polymer-grade C<sub>3</sub>H<sub>6</sub>, and the rest was

mixed with raw material and entered the column. The permeate was converted into liquified gas at 1.2 MPa by the condenser and then entered the storage tank. The feed rate was adjusted to ensure convergence of the process with recycle and the reflux ratio was optimized to meet final production specification. Our simulation results indicated that, upon setting the feed rate of the column at 15.0 kg h<sup>-1</sup>, a high reflux ratio of 11.16 with a condenser duty of 5.31 kW, a reboiler duty of 2.45 kW, and a total heater duty of 4.51 kW were required to achieve the separation target of EG C<sub>3</sub>H<sub>6</sub> with C<sub>3</sub>H<sub>6</sub> content in the permeate of 99.9987% and the recovery of 34.33% (Figure 5a, c and Table S13), equivalent to equipment cost of ~US\$1.70×10<sup>4</sup> (without considering the equipment cost of membrane) and operation cost of ~US\$5.51×10<sup>4</sup> per year.

In contrast, our model revealed that for conventional cryogenic distillation process, at least four columns are required to achieve the intended separation objective: One for removing non-condensable gas and lighter component, another for removing heavier components, and the remaining two for dual purification of C<sub>3</sub>H<sub>6</sub>. Our simulation results indicated that, with the feed rate of 7.0 kg h<sup>-1</sup> to the column, reflux ratios of 0.17, 7.33, and 8.46 for the remaining three column, respectively, along with a total condenser duty of 14.55 kW, reboiler duty of 14.37 kW, pump power of 0.0021 kW, and heater duty of 0.24 kW, 6.1 kg h<sup>-1</sup> of 99.9909% C<sub>3</sub>H<sub>6</sub> could be obtained at the top of last distillation column with the recovery of 87.57% (Figure 5b, c and Table S14). The equipment cost of the entire system was ~US\$2.12×10<sup>5</sup>, and operation cost was ~US\$1.51×10<sup>5</sup> per year. Considering the equipment cost of membrane, membrane cost below ~US\$6.45×10<sup>3</sup> m<sup>2</sup> could make the hybrid process more economically attractive than pure distillation process in terms of capital cost.

Process design analysis further demonstrated that in comparison with conventional distillation process, employing a membrane-based hybrid system with column pressure range of 2-3 bar not only enabled the production of higher quality EG C<sub>3</sub>H<sub>6</sub> with purity approaching 5N, but also could save 56.57% of operation cost (1.34 US\$ kg<sup>-1</sup> C<sub>3</sub>H<sub>6</sub>) and 49.89% of total energy duty (8.62 MJ kg<sup>-1</sup> C<sub>3</sub>H<sub>6</sub>) with potentially significant reduction in capital cost (Figure 5d and Table S15). The simulation results of operation/capital cost of the hybrid membrane-distillation systems and conventional distillation under the other two modes were compared in detail in Table S16-19. Furthermore, a parallel comparison was made of the energy-saving advantages of the membrane-distillation system that is coupled with other high-performance ZIF-8 membranes (Table S20 and S21). The proposed hybrid system

directly addresses the most critical bottleneck of EG C<sub>3</sub>H<sub>6</sub> production—the excessive energy demand of multi-column distillation for deep C<sub>3</sub>H<sub>8</sub> removal and offers a practical pathway to cost reduction and sustainability.

## Discussion

Aiming at energy-efficient and cost-saving EG C<sub>3</sub>H<sub>6</sub> production, the C<sub>3</sub>H<sub>6</sub>/C<sub>3</sub>H<sub>8</sub> separation performance of near-freezing synthetic ZIF-8 membrane was investigated under practical operation conditions. Gas permeation tests conducted at sub-freezing temperature revealed that the separation factor of this ZIF-8 membrane for an equimolar C<sub>3</sub>H<sub>6</sub>/C<sub>3</sub>H<sub>8</sub> gas mixture elevated as temperature decreases, reaching an exceptional value of 607 at -40 °C. This trend was attributed to a low-temperature-induced pore gate size reduction and ZIF-8 framework rigidification leading to a more pronounced decrease of the C<sub>3</sub>H<sub>8</sub> dynamics as compared to C<sub>3</sub>H<sub>6</sub>. Under industry-relevant operation condition of -20 °C and 3 bar, this membrane still retained a C<sub>3</sub>H<sub>6</sub>/C<sub>3</sub>H<sub>8</sub> separation factor up to 362 with polymer-grade C<sub>3</sub>H<sub>6</sub> as feedstock under vacuum operation, which enabled not only efficient stripping of C<sub>3</sub>H<sub>8</sub> impurity from 2998 to 8 ppm but also complete removal of n-/i-C<sub>4</sub>H<sub>10</sub> impurities, achieving direct coupling between membrane unit and de-light column under identical operation conditions. Furthermore, a hybrid membrane-distillation system was established based on above membrane. Process design analysis demonstrated that in comparison with conventional cryogenic distillation, the ZIF-8 membrane-distillation system not only enabled the production of high-standard EG C<sub>3</sub>H<sub>6</sub> (~5N) but also achieved significant savings in operation cost and total energy duty (56.57% and 49.89%), thereby holding great promise in energy-efficient and cost-saving EG C<sub>3</sub>H<sub>6</sub> production under practical conditions.

## Methods

### Preparation of ZIF-8 membrane

ZIF-8 membrane was prepared through near-freezing conversion of ZnO buffer layer. The first step involved surface deposition of porous α-Al<sub>2</sub>O<sub>3</sub> substrate with ZnO buffer layer through sequential spin-coating of ZIF-8 nanocrystals and ZnO sol, followed by calcination at 450 °C for 2 h. The second step referred to ZIF-8 membrane synthesis through near-freezing conversion of obtained ZnO buffer layer. The precursor solution was prepared by dissolving Zn(OAc)<sub>2</sub> (0.23 mmol) and 2-mIm (41.67 mmol) in 50 ml of methanol-water (v/v=3/7) binary solvent. ZnO layer-modified substrate was then immersed in above pre-cooled solution at 2.5 °C for 24 h to form well-intergrown ZIF-8 membrane. The relevant characteristics, gas permeation

tests and information on reagent purity are provided in Supplementary Methods.

### Adsorption and diffusion studies

The ideal adsorbed solution theory (IAST) was used to calculate C<sub>3</sub>H<sub>6</sub>/C<sub>3</sub>H<sub>8</sub> adsorption selectivity. Gas adsorption isotherms were fitted by *Langmuir* (Equation 1) and *Dual-site Langmuir* (Equation 2) models:

$$q = q_m \frac{bp}{1 + bp} \quad (1)$$

$$q = q_{m1} \frac{b_1 p}{1 + b_1 p} + q_{m2} \frac{b_2 p}{1 + b_2 p} \quad (2)$$

where  $q_{m1}$  and  $q_{m2}$  (mmol g<sup>-1</sup>) were the saturated adsorption amounts at different adsorption sites, and  $b_1$  and  $b_2$  (kPa<sup>-1</sup>) were the gas affinity coefficients at different adsorption sites,  $p$  (kPa) was the adsorption pressure. The IAST ideal adsorption selectivity was calculated using the Equation 3:

$$S_{ads} = \frac{q_a/q_b}{p_a/p_b} \quad (3)$$

where  $q_1$  and  $q_2$  (mmol g<sup>-1</sup>) were the adsorbed amounts of component  $a$  and  $b$ ,  $p_1$  and  $p_2$  (kPa) were the adsorption pressures of component  $a$  and  $b$ . The heats of adsorption ( $Q_{st}$ ) for C<sub>3</sub>H<sub>6</sub> and C<sub>3</sub>H<sub>8</sub> were calculated using the Clausius-Clapeyron Equation 4-5:

$$Q_{st} = -RT^2 \left( \frac{\partial \ln p}{\partial T} \right) n_i \quad (4)$$

$$\ln p = \frac{Q_{st}}{RT} + C \quad (5)$$

where  $T$  (K) was measured temperature,  $R$  (8.314 J mol<sup>-1</sup> K<sup>-1</sup>) was the gas constant, and  $n_i$  (mmol g<sup>-1</sup>) was the amount of adsorption. Based on adsorption-diffusion transport mechanism of gas within porous molecular sieve membrane, the gas flux could be expressed by the adsorption and diffusion coefficients in Equation 6:

$$F_a = \phi \rho D_c \int_{q_f}^{q_p} \frac{d \ln p}{d \ln q} dp \quad (6)$$

where  $F_a$  (mol m<sup>-2</sup> s<sup>-1</sup>) was the permeate flux of component  $a$ ,  $\rho$  (g cm<sup>-3</sup>) was the density of ZIF-8,  $\phi$  was the ratio of the porosity to the curvature of ZIF-8,  $D_c$  (cm<sup>2</sup> s<sup>-1</sup>) was the diffusion coefficient of component  $a$ ,  $q_f$  and  $q_p$  were the concentration of component  $a$  on the feed and permeate side. The flux-pressure relationship could be obtained by inserting Equation 1 and 2 to 6:

$$F_a = \frac{\phi \rho D_c}{L} q_m \ln(1 + bp_f) \quad (7)$$

$$F_a = \frac{\phi \rho D_c}{L} [q_{m1} \ln(1 + b_1 p_f) + q_{m2} \ln(1 + b_2 p_f)] \quad (8)$$

where the  $L$  (μm) was the thickness of the ZIF-8

membrane and the  $p_f$  (kPa) was partial pressure of gas  $a$  in the feed side.

### MD simulation

The LAMMPS (7 Aug 2019) software<sup>69-70</sup> was employed to perform the MD simulations considering a simulation box of  $2 \times 2 \times 2$  ZIF-8 unit cells (2208 atoms) at different temperatures. The verlet-velocity integration algorithm with a time step of 1.0 fs was used. The force field parameters for the flexible ZIF-8 framework, i.e., bonding, van der Waals, and electrostatic interactions, were taken from previous works<sup>71-72</sup>. All non-bonded interactions were calculated using a cut-off of 12.0 Å. For each investigated temperature, the system was equilibrated at a constant temperature and 1 bar pressure for 10 ns using an isothermal–isobaric ensemble (*NPT*) with Nosé–Hoover model. Relaxation times were set as  $\tau_T = 1.0$  ps and  $\tau_P = 5.0$  ps. The largest cylinder which could pass through the gate was employed to evaluate the gate size of ZIF-8 while the swing angle value was determined following the same methodology we applied earlier<sup>73</sup>.

### Process simulation

Process simulations for hybrid membrane-distillation system and multi-column distillation system were conducted with steady-state simulation model developed in Aspen Plus V11 software. The hybrid membrane-distillation system mainly consisted of a distillation column and a membrane unit. The total number of trays in the distillation column was set to 9 with the feed entering from tray 4. Liquid N<sub>2</sub> was used as cooling utility agent in the condenser, where chilled water was used as heating utility agent in the reboiler. Membrane unit was simulated with the standard component separator model, and separation parameters were determined by experimental data of gas permeation test. The conventional cryogenic distillation system consisted of 4 tandem distillation columns with the tray number of 9, 24, 102 and 106, and feeds were introduced from tray 4, 11, 37 and 37, respectively. The relevant information on economic analyses can be found in Supplementary Methods.

### Data availability

The data that support the findings of this study are provided in the main manuscript or within the Supplementary Information. Source data are provided with this paper.

### References

- Compagnoni, C. M. et al., Reviewing the Evolution of the NAND Flash Technology. *P. IEEE*. **105**, 1609-1633 (2017).
- Goda, A., Recent Progress on 3D NAND Flash Technologies. *Electronics* **10**, 3156 (2021).
- Kim, I. et al., Amorphous Carbon Films for Electronic Applications. *Adv. Mater.* **35**, 2204912 (2023).
- Ghoshal, T. et al., Fabrication of Graphoepitaxial Gate-All-Around Si Circuitry Patterned Nanowire Arrays Using Block Copolymer Assisted Hard Mask Approach. *ACS Nano* **15**, 9550-9558 (2021).
- Jiang, Z., Zhu, H. & Sun, Q., Process Optimization of Amorphous Carbon Hard Mask in Advanced 3D-NAND Flash Memory Applications. *Electronics* **10**, 1374 (2021).
- Nagasawa, H., Kanezashi, M., Yoshioka, T. & Tsuru, T., Plasma-enhanced chemical vapor deposition of amorphous carbon molecular sieve membranes for gas separation. *RSC Adv.* **6**, 59045-59049 (2016).
- Wang, J., Park, J., Lu, A. & Kong, J., Electrical Control of Chemical Vapor Deposition of Graphene. *J. Am. Chem. Soc.* **144**, 22925-22932 (2022).
- Fairbairn, K. et al., Method for Depositing an Amorphous Carbon Layer. US 6573030B1 (2003).
- Phung, T. K., Le Minh Pham, T., Vu, K. B. & Busca, G., (Bio)Propylene production processes: A critical review. *J. Environ. Chem. Eng.* **9**, 105673 (2021).
- Agarwal, A., Sengupta, D. & El-Halwagi, M., Sustainable Process Design Approach for On-Purpose Propylene Production and Intensification. *ACS Sustain. Chem. Eng.* **6**, 2407-2421 (2018).
- Sholl, D. S. & Lively, R. P., Seven chemical separations to change the world. *Nature* **532**, 435-437 (2016).
- Ding, Q. & Zhang, S., Recent Advances in the Development of Metal-Organic Frameworks for Propylene and Propane Separation. *Energ. Fuel.* **36**, 7337-7361 (2022).
- Qian, Q. et al., MOF-Based Membranes for Gas Separations. *Chem. Rev.* **120**, 8161-8266 (2020).
- Antypov, D. et al., Differential guest location by host dynamics enhances propylene/propane separation in a metal-organic framework. *Nat. Commun.* **11**, 6099 (2020).
- Reddy, A. S., Sharda, P., Nehra, S. P. & Sharma, A., Advanced strategies in MOF-based mixed matrix membranes for propylene /propane separation: A critical review. *Coordin. Chem. Rev.* **498**, 215435 (2024).
- Yuan, Y. et al., Wiggling Mesopores Kinetically Amplify the Adsorptive Separation of Propylene/Propane. *Angew. Chem. Int. Ed.* **60**, 19063-19067 (2021).
- Qiu, W. et al., Surprising olefin/paraffin separation performance recovery of highly aged carbon molecular sieve hollow fiber membranes by a super-hyperaging treatment. *J. Membr. Sci.* **620**, 118701 (2021).
- Yang, K., Ban, Y. & Yang, W., Layered MOF membranes modified with ionic liquid/AgBF<sub>4</sub> composite for olefin/paraffin separation. *J. Membr. Sci.* **639**, 119771 (2021).
- Li, K. et al., Zeolitic Imidazolate Frameworks for Kinetic Separation of Propane and Propene. *J. Am. Chem. Soc.*

- 131**, 10368-10369 (2009).
20. Freund, R. et al., The Current Status of MOF and COF Applications. *Angew. Chem. Int. Ed.* **60**, 23975-24001 (2021).
  21. Liu, Y., Ban, Y. & Yang, W., Microstructural Engineering and Architectural Design of Metal-Organic Framework Membranes. *Adv. Mater.* **29**, 1606949 (2017).
  22. Dou, H. et al., Microporous framework membranes for precise molecule/ion separations. *Chem. Soc. Rev.* **50**, 986-1029 (2021).
  23. Park, H. B., Kamcev, J., Robeson, L. M., Elimelech, M. & Freeman, B. D., Maximizing the right stuff: The trade-off between membrane permeability and selectivity. *Science* **356**, 1137 (2017).
  24. Cadiau, A., Adil, K., Bhatt, P. M., Belmabkhout, Y. & Eddaoudi, M., A metal-organic framework-based splitter for separating propylene from propane. *Science* **353**, 137-140 (2016).
  25. Xue, D. et al., Tunable Rare Earth fcu-MOF Platform: Access to Adsorption Kinetics Driven Gas/Vapor Separations via Pore Size Contraction. *J. Am. Chem. Soc.* **137**, 5034-5040 (2015).
  26. Pan, Y., Li, T., Lestari, G. & Lai, Z., Effective separation of propylene/propane binary mixtures by ZIF-8 membranes. *J. Membr. Sci.* **390**, 93-98 (2012).
  27. Lai, Z., Development of ZIF-8 membranes: opportunities and challenges for commercial applications. *Curr. Opin. Chem. Eng.* **20**, 78-85 (2018).
  28. Alshehri, A. & Lai, Z., Attainability and minimum energy of single-stage membrane and membrane/distillation hybrid processes. *J. Membr. Sci.* **472**, 272-280 (2014).
  29. Hou, J. et al., Olefin/paraffin separation through membranes: from mechanisms to critical materials. *J. Mater. Chem. A* **7**, 23489-23511 (2019).
  30. Roy, A. et al., Membranes for olefin-paraffin separation: An industrial perspective. *P. Natl. Acad. Sci. USA* **118**, e2022194118 (2021).
  31. Peterson, G. W., Lee, D. T., Barton, H. F., Epps, T. H. & Parsons, G. N., Fibre-based composites from the integration of metal-organic frameworks and polymers. *Nat. Rev. Mater.* **6**, 605-621 (2021).
  32. Lang, L., Banihashemi, F., James, J. B., Miao, J. & Lin, J. Y. S., Enhancing selectivity of ZIF-8 membranes by short-duration postsynthetic ligand-exchange modification. *J. Membr. Sci.* **619**, 118743 (2021).
  33. Yang, L. et al., Energy-efficient separation alternatives: metal-organic frameworks and membranes for hydrocarbon separation. *Chem. Soc. Rev.* **49**, 5359-5406 (2020).
  34. Chen, T., Li, H., Shi, X., Imbrogno, J. & Zhao, D., Robust Homochiral Polycrystalline Metal-Organic Framework Membranes for High-Performance Enantioselective Separation. *J. Am. Chem. Soc.* **146**, 14433-14438 (2024).
  35. Wang, F. et al., Hydrophobic ultrathin MOF membranes with tuning pore structure for efficient alcohol-permselective pervaporation. *J. Membr. Sci.* **698**, 122615 (2024).
  36. Liu, G. et al., Eliminating lattice defects in metal-organic framework molecular-sieving membranes. *Nat. Mater.* **22**, 769-776 (2023).
  37. Kadioglu, O. & Keskin, S., Efficient separation of helium from methane using MOF membranes. *Sep. Purif. Technol.* **191**, 192-199 (2018).
  38. Zhou, S. et al., Asymmetric pore windows in MOF membranes for natural gas valorization. *Nature* **606**, 706-712 (2022).
  39. Zeng, H. et al., Orthogonal-array dynamic molecular sieving of propylene/propane mixtures. *Nature* **595**, 542-548 (2021).
  40. Kwon, H. T. & Jeong, H., In Situ Synthesis of Thin Zeolitic-Imidazolate Framework ZIF-8 Membranes Exhibiting Exceptionally High Propylene/Propane Separation. *J. Am. Chem. Soc.* **135**, 10763-10768 (2013).
  41. Eum, K. et al., Fluidic Processing of High-Performance ZIF-8 Membranes on Polymeric Hollow Fibers: Mechanistic Insights and Microstructure Control. *Adv. Funct. Mater.* **26**, 5011-5018 (2016).
  42. Tu, S. et al., A new yttrium-based metal-organic framework for molecular sieving of propane from propylene with high propylene capacity. *AIChE J.* **68**, e17551 (2022).
  43. Bux, H. et al., Zeolitic Imidazolate Framework Membrane with Molecular Sieving Properties by Microwave-Assisted Solvothermal Synthesis. *J. Am. Chem. Soc.* **131**, 16000-16001 (2009).
  44. Lee, M. J. et al., Ultrathin zeolitic-imidazolate framework ZIF-8 membranes on polymeric hollow fibers for propylene/propane separation. *J. Membr. Sci.* **559**, 28-34 (2018).
  45. Hamid, M. R. A., Park, S., Kim, J. S., Lee, Y. M. & Jeong, H., Synthesis of Ultrathin Zeolitic Imidazolate Framework ZIF-8 Membranes on Polymer Hollow Fibers Using a Polymer Modification Strategy for Propylene/Propane Separation. *Ind. Eng. Chem. Res.* **58**, 14947-14953 (2019).
  46. Wei, T. et al., Rapid mechanochemical encapsulation of biocatalysts into robust metal-organic frameworks. *Nat. Commun.* **10**, 5002 (2019).
  47. Brown, A. J. et al., Interfacial microfluidic processing of metal-organic framework hollow fiber membranes. *Science* **345**, 72-75 (2014).
  48. Lee, M. J., Kwon, H. T. & Jeong, H., High-Flux Zeolitic Imidazolate Framework Membranes for Propylene/Propane Separation by Postsynthetic Linker Exchange. *Angew. Chem. Int. Ed.* **57**, 156-161 (2018).
  49. Huang, K., Dong, Z., Li, Q. & Jin, W., Growth of a ZIF-8 membrane on the inner-surface of a ceramic hollow fiber via cycling precursors. *Chem. Commun.* **49**, 10326-

- 10328 (2013).
50. Ma, X. et al., Zeolitic imidazolate framework membranes made by ligand-induced permselectivation. *Science* **361**, 1008-1011 (2018).
  51. Marreiros, J. et al., Vapor-Phase Linker Exchange of the Metal-Organic Framework ZIF-8: A Solvent-Free Approach to Post-synthetic Modification. *Angew. Chem. Int. Ed.* **58**, 18471-18475 (2019).
  52. Miao, Y. et al., Solvent-free bottom-up patterning of zeolitic imidazolate frameworks. *Nat. Commun.* **13**, 420 (2022).
  53. Zhou, S. et al., Paralyzed membrane: Current-driven synthesis of a metal-organic framework with sharpened propene/propane separation. *Sci. Adv.* **4**, eaau1393 (2018).
  54. Park, K. S. et al., Exceptional chemical and thermal stability of zeolitic imidazolate frameworks. *P. Natl. Acad. Sci. USA* **103**, 10186-10191 (2006).
  55. Lian, H. et al., Controllable synthesis of ZIF-8 interlocked membranes for propylene/propane separation. *Sep. Purif. Technol.* **300**, 121811 (2022).
  56. Stassen, I. et al., Chemical vapour deposition of zeolitic imidazolate framework thin films. *Nat. Mater.* **15**, 304-319 (2016).
  57. Ji, T. et al., Towards ZIF-8 membranes with superb C<sub>3</sub>H<sub>6</sub>/C<sub>3</sub>H<sub>8</sub> separation performances under varying conditions: Necessity of precise temperature control. *J. Membr. Sci.* **683**, 121776 (2023).
  58. Ji, T. et al., Sub-Zero Temperature Synthesis of Pressure-Resistant ZIF-8 Membrane with Superior C<sub>3</sub>H<sub>6</sub>/C<sub>3</sub>H<sub>8</sub> Separation Performance. *ACS Mater. Lett.* **4**, 1094-1100 (2022).
  59. Ji, T. et al., Subfreezing conversion of ALD-derived ZnO layer to ultra-thin ZIF-8 membrane for high-flux C<sub>3</sub>H<sub>6</sub> production. *Chem. Eng. Sci.* **282**, 119293 (2023).
  60. Liu, D., Ma, X., Xi, H. & Lin, Y. S., Gas transport properties and propylene/propane separation characteristics of ZIF-8 membranes. *J. Membrane. Sci.* **451**, 85-93 (2014).
  61. Ma, Q. et al., Ultrafast Semi-Solid Processing of Highly Durable ZIF-8 Membranes for Propylene/Propane Separation. *Angew. Chem. Int. Ed.* **59**, 21909-21914 (2020).
  62. Kumari, G., Jayaramulu, K., Maji, T. K. & Narayana, C., Temperature Induced Structural Transformations and Gas Adsorption in the Zeolitic Imidazolate Framework ZIF-8: A Raman Study. *J. Phys. Chem. A* **117**, 11006-11012 (2013).
  63. Morris, W. et al., NMR and X-ray Study Revealing the Rigidity of Zeolitic Imidazolate Frameworks. *J. Phys. Chem. C* **116**, 13307-13312 (2012).
  64. Kwon, H. T., Jeong, H.-K., Lee, A. S., An, H. S. & Lee, J. S. Heteroepitaxially Grown Zeolitic Imidazolate Framework Membranes with Unprecedented Propylene/Propane Separation Performances. *J. Am. Chem. Soc.* **137**, 12304-12311 (2015).
  65. Liu, Y. et al. MOF-COF "Alloy" Membranes for Efficient Propylene/Propane Separation. *Adv. Mater.* **34**, 2201423 (2022).
  66. Zhou, S. et al., Electrochemical synthesis of continuous metal-organic framework membranes for separation of hydrocarbons. *Nat. Energy* **6**, 882-891 (2021).
  67. Lee, U., Kim, J., Chae, I. S. & Han, C., Techno-economic feasibility study of membrane based propane/propylene separation process. *Chem. Eng. Process.* **119**, 62-72 (2017).
  68. Yamaki, T. et al., Impact of process configuration on energy consumption and membrane area in hybrid separation process using olefin-selective zeolite membrane. *Sep. Purif. Technol.* **294**, 121208 (2022).
  69. <http://lammps.sandia.gov>.
  70. Plimpton, S. Fast Parallel Algorithms for Short-range Molecular-dynamics. *J. Comput. Phys.* **117**, 1-19 (1995).
  71. Zheng, B., Pan, Y., Lai, Z. & Huang, K.-W. Molecular Dynamics Simulations on Gate Opening in ZIF-8: Identification of Factors for Ethane and Propane Separation. *Langmuir* **29**, 8865-8872 (2013).
  72. Zheng, B., Sant, M., Demontis, P. & Suffritti, G. B. Force Field for Molecular Dynamics Computations in Flexible ZIF-8 Framework. *J. Phys. Chem. C* **116**, 933-938 (2012).
  73. Zheng, B. & Maurin, G. Mechanical Control of the Kinetic Propylene/Propane Separation by Zeolitic Imidazolate Framework-8. *Angew. Chem. Int. Ed.* **58**, 13734-13738 (2019).

## Acknowledgements

G.M. thanks IUF for the Senior Chair.

## Funding

The authors gratefully acknowledge the financial support of the National Key Research and Development Program of China (2023YFB3810700 to Y.L.), the Science Fund for Creative Research Groups of the National Natural Science Foundation of China (22021005 to Y.L.), the National Natural Science Foundation of China (22478056 to Y.L., 22078039 to Y.L.), the Science and Technology Innovation Fund of Dalian (2024JJ12GX027 to Y.L.) and the Fundamental Research Funds for the Central Universities (DUT22LAB602 to Y.L.). The authors would like to appreciate the HPC resources provided by GENCI-CINES (A0160907613 to G.M.).

## Author contributions

Y.L. conceived the idea, designed the experiment, obtained the funding, supervised students, and revised the manuscript. K.Y. and T.J. carried out the experiment and drafted the manuscript. Y.D. and S.G. performed the process simulation. B.Z. and G.M.

performed the MD simulation. J.L., J.W. and Y.G. analyzed the in situ FT-IR data. J.Y. and X.H. contributed to the review of the manuscript. All authors contributed to the manuscript.

**Competing interests**

The authors declare no competing interests.

**Editorial Summary:**

Purifying electronic-grade propylene is challenging due to trace impurities. Here, authors demonstrate a ZIF-8 membrane that efficiently removes impurities at low temperatures, enabling high-purity propylene production with reduced energy and cost.

**Peer review information:** *Nature Communications* thanks Yun-Lei Peng, Inmaculada Ortiz and the other, anonymous, reviewer(s) for their contribution to the peer review of this work. A peer review file is available.